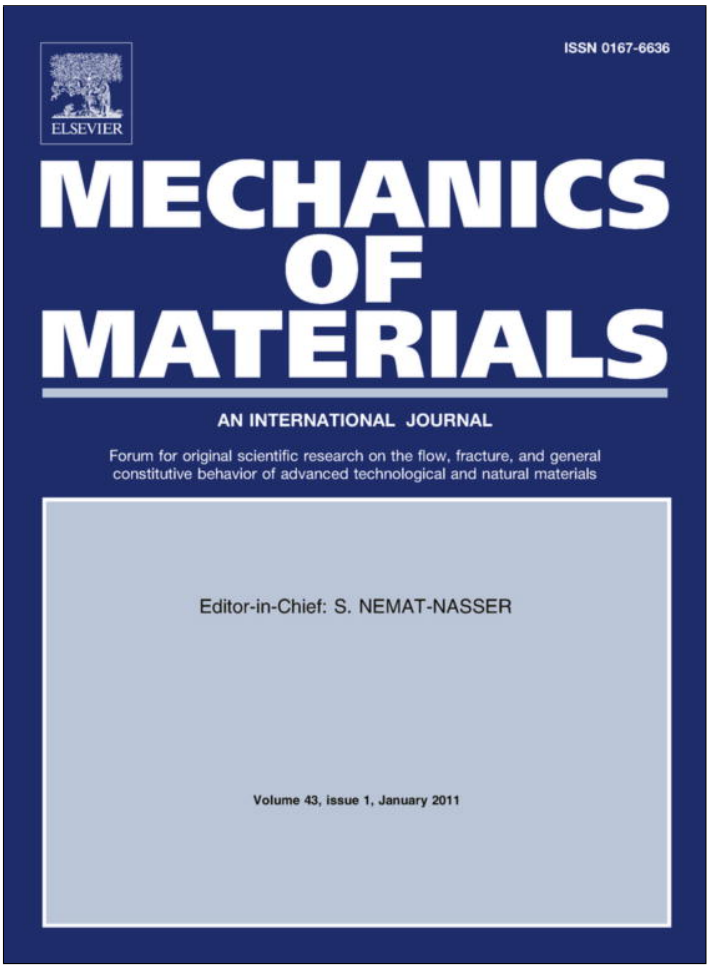

(This is a sample cover image for this issue. The actual cover is not yet available at this time.)

Mechanics of Materials 43 (2011) 627–642

Contents lists available at SciVerse ScienceDirect

Mechanics of Materials

journal homepage: www.elsevier.com/locate/mechmat

Concomitant wrinkling and buckle-delamination of elastic thin films on compliant substrates

Haixia Mei, Chad M. Landis, Rui Huang *

Department of Aerospace Engineering and Engineering Mechanics, University of Texas, Austin, TX 78712, USA

ARTICLE INFO

Article history:
Received 15 March 2011
Received in revised form 22 July 2011
Available online 16 August 2011

Keywords:
Wrinkling
Buckling
Delamination
Thin film
Compliant substrate

ABSTRACT

Compressing a thin elastic film attached to a thick compliant substrate can lead to buckling instability. Two commonly observed buckling modes, buckle-delamination and wrinkling, have each been analyzed separately in previous studies. Recent experiments have observed that the two modes can co-exist and co-evolve. In this paper, by analytical and finite element methods, we present a study on concomitant wrinkling and buckle-delamination for an elastic film on a highly compliant substrate. First, without delamination, we present an analytical solution for wrinkling that takes into account the effect of Poisson's ratio of the substrate. In comparison with a nonlinear finite element analysis, an approximate formula is derived to estimate the normal traction at the interface and to predict initiation of wrinkle-induced delamination. Next, with a pre-existing delamination crack, the critical strain for the onset of buckling instability is predicted by finite element eigenvalue analysis. For an intermediate delamination size, a mixed buckling mode is predicted with the critical compressive strain lower than previous solutions for both wrinkling and buckle-delamination. Post-buckling analyses show a significant shear-lag effect with an effective load transfer length three orders of magnitude greater than the film thickness. Finally, concomitant wrinkling and buckle-delamination is simulated to illustrate the interaction between the two buckling modes, and the results are discussed in view of failure mechanisms and applications in thin film metrology.

1. Introduction

Stiff thin films on compliant substrates are used in a wide range of technological applications, including flexible electronics (Lacour et al., 2005; Rogers et al., 2010), thin film metrology (Chung et al., 2011), and micro/nano-fabrication (Bowden et al., 1998). Similar material structures are abundant in nature (Genzer and Groenewold, 2006; Chen and Yin, 2010). The mechanical interaction between a stiff film and a compliant substrate leads to a rich variety of phenomena that either limit or inspire practical applications of the hybrid system integrating hard and soft materials. For example, early adoption of stiff skin layers in sandwich panels for aircraft structures had motivated studies of compression-induced buckling and surface wrinkling as potential failure mechanisms (Biot, 1957; Allen, 1969). Recent interests in micro/nano-scale thin film materials have exploited the mechanical instability as an enabling mechanism for novel applications (e.g., Watanabe et al., 2002; Harrison et al., 2004; Chan et al., 2008, 2009). Meanwhile, mechanics of surface wrinkling has been studied extensively over the last decade (e.g., Shield et al., 1994; Groenewold, 2001; Huang and Suo, 2002; Chen and Hutchinson, 2004; Huang and Im, 2006; Jiang et al., 2007; Lee et al., 2008; Audoly and Boudaoud, 2008; Im and Huang, 2008; Sun et al., submitted for publication; Cai et al., 2011). While most of these studies have assumed perfect bonding between the film and the substrate, it has been occasionally pointed out that wrinkling may cause interfacial delamination (Shield et al., 1994; Liang et al., 2002; Mei et al., 2007; Bazant and Grassl,

* Corresponding author.
E-mail address: ruihuang@mail.utexas.edu (R. Huang).

0167-6636/$ - see front matter © 2011 Elsevier Ltd. All rights reserved.
doi:10.1016/j.mechmat.2011.08.003

2007; Goyal et al., 2010). On the other hand, interfacial delamination is a necessary condition for buckling of thin films attached to relatively stiff substrates (Hutchinson and Suo, 1992; Ortiz and Gioia, 1997; Moon et al., 2002). Simultaneous buckling and delamination has also been observed in compressed thin films on compliant substrates (Cotterell and Chen, 2000; Parry et al., 2005; Vella et al., 2009). More recently, some experiments have shown both surface wrinkling and buckle-delamination co-existing in the same film/substrate system (Mei et al., 2007; Nolte et al., submitted for publication).

The characteristics of the two buckling modes are often observable, with localized patterns for buckle-delamination and periodic patterns for surface wrinkling, as illustrated in Fig. 1. In a previous work (Mei et al., 2007), we proposed a quantitative criterion for selection of the initial buckling mode by comparing the critical conditions for surface wrinkling and buckle-delamination. The favored buckling mode at the onset of instability depends on the elastic mismatch between the film and the substrate as well as on the size of pre-existing interfacial delamination. In this paper, we present a study on concomitant wrinkling and buckle-delamination for an elastic thin film on a very compliant substrate beyond the initial stage of buckling instability.

The remainder of this paper is organized as follows. Section 2 presents an analytical solution and finite element analysis for wrinkling with no delamination, based on which an approximate formula is derived to estimate the normal traction at the interface and to predict initiation of wrinkle-induced delamination. In Section 3, a finite element eigenvalue analysis is performed to predict the effect of pre-existing interfacial delamination on the critical condition for onset of buckling instability as well as the buckling mode. Nonlinear post-buckling analysis is presented in Section 4, emphasizing the long-range interaction via the compliant substrate and demonstrating concomitant buckling modes. Section 5 discusses implications of the present results on prediction of failure mechanisms and thin film metrology.

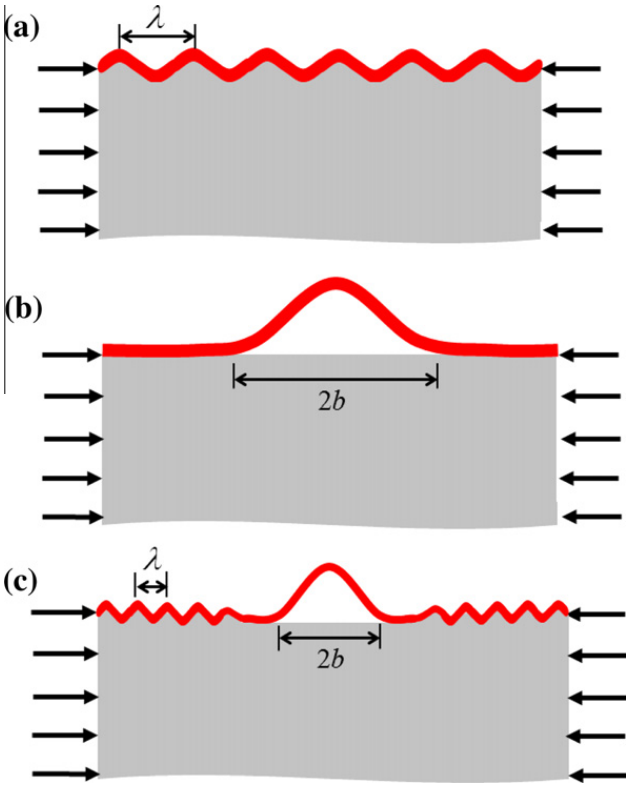

Fig. 1. Schematic illustration of buckling modes for an elastic thin film on a compliant substrate. (a) Surface wrinkling with no delamination; (b) buckle-delamination; (c) concomitant wrinkling and buckle-delamination.

2. Wrinkling, with no delamination

2.1. Analytical solutions

Consider an elastic thin film on an elastic compliant substrate, subject to lateral compression. Both the film and the substrate are taken to be linear elastic and isotropic, restricted to small, plane-strain deformation for the present study. Let ε be the nominal compressive strain, relative to the stress-free state. When ε is relatively small, the film/substrate bilayer is uniformly compressed and the surface is flat. When the strain exceeds a critical value, the film buckles and the substrate deforms coherently, forming surface wrinkles (Fig. 1a). The interface between the film and the substrate is assumed to be perfectly bonded in this section, and the effect of interfacial delamination will be discussed in Section 3. Let h be the thickness of the film, while the substrate is considered infinitely thick. A well-known analytical solution predicts the critical strain for onset of wrinkling (Chen and Hutchinson, 2004; Huang et al., 2005):

$$\varepsilon_c(kh) = \frac{(kh)^2}{12} + \frac{1}{2kh}\frac{\bar{E}_s}{\bar{E}_f}, \tag{1}$$

where k is the wave number so that $\lambda = 2\pi/k$ is the wrinkle wavelength, $\bar{E} = E/(1-\nu^2)$ is the plane-strain modulus with E for Young's modulus and ν for Poisson's ratio, and the subscripts f and s denote the film and substrate, respectively.

For a given ratio, $\bar{E}_s/\bar{E}_f$, the critical strain in (1) minimizes at a particular wavelength,

$$\lambda^* = 2\pi h\left(\frac{\bar{E}_f}{3\bar{E}_s}\right)^{1/3}, \tag{2}$$

and the corresponding critical strain is

$$\varepsilon_c^* = \frac{1}{4}\left(\frac{3\bar{E}_s}{\bar{E}_f}\right)^{2/3}. \tag{3}$$

In deriving the above analytical solution, the shear traction at the film/substrate interface was assumed to be zero. Alternatively, by assuming zero tangential displacement at the interface, a similar analytical solution can be obtained (Huang, 2005; Audoly and Boudaoud, 2008). The two solutions are identical if the substrate is incompressible ($\nu_s = 0.5$), in which case both the shear traction and tangential displacement are zero. However, when the substrate is

compressible ($\nu_s < 0.5$), neither the shear traction nor the tangential displacement is zero at the interface as the film wrinkles. As a result, neither analytical solution accurately accounts for the effect of Poisson's ratio of the substrate, which could cause considerable errors in prediction of the critical strain as well as subsequent evolution of wrinkles (Cai et al., 2011). Here we present a more accurate analytical solution, taking into account both the shear traction and the tangential displacement at the interface.

The deformation of the thin film is described by the linear plate equations, which are sufficient for linear perturbation analysis to predict the critical condition for onset of wrinkling. Assume a small perturbation with normal deflection (w) and tangential displacement (u) in the film. The equilibrium condition of the film requires that

$$q = -\frac{\bar{E}_f h^3}{12}\frac{d^4 w}{dx^4} + \varepsilon \bar{E}_f h \frac{d^2 w}{dx^2}, \tag{4}$$

$$\tau = \bar{E}_f h \frac{d^2 u}{dx^2}, \tag{5}$$

where q and τ are the normal and shear tractions at the film/substrate interface, respectively.

Both the displacements and the tractions are assumed to be continuous across the interface. Consequently, in addition to (4) and (5), they are related to each other by the equilibrium condition for the substrate. Assume a pair of periodic tractions, $\tau = \tau_m \sin(kx)$ and $q = q_m \cos(kx)$, acting on the surface of an infinitely thick substrate. By solving the equations of linear elasticity under the plane-strain condition (Huang, 2005), the surface displacements of the substrate are obtained as

$$u(x) = \frac{1}{k\bar{E}_s}\left[2\tau_m + \frac{1-2\nu_s}{1-\nu_s} q_m\right] \sin(kx), \tag{6}$$

$$w(x) = \frac{1}{k\bar{E}_s}\left[\frac{1-2\nu_s}{1-\nu_s}\tau_m + 2q_m\right] \cos(kx). \tag{7}$$

Inserting (6) and (7) into (4) and (5) results in a linear eigenvalue problem, namely

$$\left(\frac{\bar{E}_s}{\bar{E}_f}\frac{1}{kh} + 2\right)\tau_m + \frac{1-2\nu_s}{1-\nu_s} q_m = 0, \tag{8}$$

$$\frac{1-2\nu_s}{1-\nu_s}\tau_m + \left[\frac{\bar{E}_s}{\bar{E}_f}\left(\frac{1}{12}(kh)^3 + \varepsilon kh\right)^{-1} + 2\right] q_m = 0. \tag{9}$$

By setting the determinant of the coefficient matrix in (8) and (9) to zero, we obtain the critical strain for wrinkling as a function of kh,

$$\varepsilon_c(kh) = \frac{(kh)^2}{12} + \frac{1}{2kh}\left(\frac{\bar{E}_s}{\bar{E}_f}\right)\left[1 - \frac{1}{2}\left(\frac{1-2\nu_s}{1-\nu_s}\right)^2 \left(\frac{\bar{E}_s}{\bar{E}_f}\frac{1}{kh} + 2\right)^{-1}\right]^{-1}. \tag{10}$$

For a very compliant substrate, assuming $\bar{E}_s/\bar{E}_f << 2kh$, the critical strain in (10) is approximately

$$\varepsilon_c(kh) \approx \frac{(kh)^2}{12} + \frac{1}{2kh}\left(\frac{\bar{E}_s}{\bar{E}_f}\right)\left[1 - \frac{1}{4}\left(\frac{1-2\nu_s}{1-\nu_s}\right)^2\right]^{-1}. \tag{11}$$

Both (10) and (11) reduce to (1) when $\nu_s = 0.5$.

The critical strain in (11) is minimized at a particular wavelength

$$\lambda^{**} = 2\pi h\left(\frac{\bar{E}_f}{3\bar{E}_s}\right)^{1/3}\left[1 - \frac{1}{4}\left(\frac{1-2\nu_s}{1-\nu_s}\right)^2\right]^{1/3}, \tag{12}$$

and the corresponding minimum critical strain is

$$\varepsilon_c^{**} = \frac{1}{4}\left(\frac{3\bar{E}_s}{\bar{E}_f}\right)^{2/3}\left[1 - \frac{1}{4}\left(\frac{1-2\nu_s}{1-\nu_s}\right)^2\right]^{-2/3}. \tag{13}$$

Fig. 2 shows the effect of Poisson's ratio (ν_s) on the critical strain and the wrinkle wavelength, comparing the analytical solutions in (12) and (13) with those in (2) and (3). As ν_s increases, the ratio between the two critical strains, $\varepsilon_c^{**}/\varepsilon_c^{*}$, decreases, while the ratio between the two wrinkle wavelengths, λ^{**}/λ^{*}, increases. For an incompressible substrate ($\nu_s = 0.5$), both ratios are identically one. For a compressible substrate ($\nu_s < 0.5$), however, Eq. (3) underestimates the critical strain and Eq. (2) overestimates the

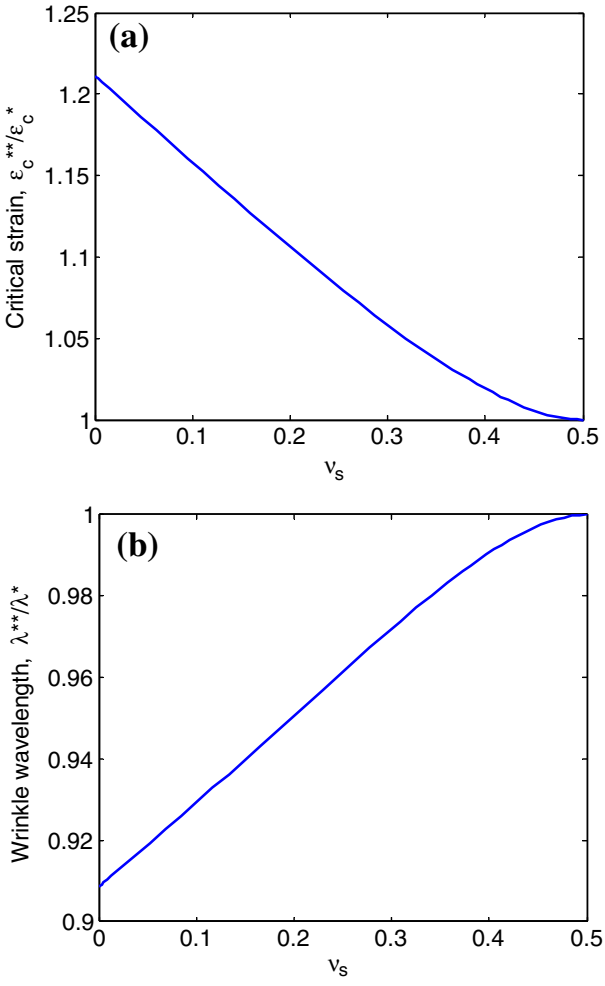

Fig. 2. Effects of the substrate Poisson's ratio on wrinkling: (a) critical strain for onset of wrinkling; (b) wrinkle wavelength.

wrinkle wavelength. The difference can be significant, up to about 20% for the critical strain and nearly 10% for the wavelength.

Beyond the critical strain, the wrinkle amplitude grows as a function of the nominal strain ε. An approximate solution for the wrinkle amplitude was obtained previously by a nonlinear approach that minimizes the strain energy in the film and the substrate (Huang, 2005; Huang et al., 2005). For an arbitrary wavelength (λ), the equilibrium wrinkle amplitude is

$$A_W(\lambda) = \frac{\lambda}{\pi}\sqrt{\varepsilon - \varepsilon_c}. \tag{14}$$

When the wavelength $\lambda = \lambda^*$, the equilibrium amplitude becomes

$$A_W^* = h\sqrt{\frac{\varepsilon}{\varepsilon_c^*} - 1}. \tag{15}$$

Apparently, using an underestimated critical strain would result in an overestimate of the wrinkle amplitude by (14), (15). Thus, the prediction of wrinkle amplitude should also take into account the effect of substrate Poisson's ratio, which however is beyond the analytical approach.

2.2. Finite element analysis of wrinkling

Next we present results from finite element analysis (FEA) of wrinkling, in comparison with the analytical solutions. As illustrated in Fig. 3, a two-dimensional (2D) plane-strain model is constructed using the commercial FEA package, ABAQUS. Besides the film thickness h, the thickness of the substrate is H and the length is L in the FEA model. The effects of H and L on the results will be discussed. The pre-existing delamination size b is set to zero for the wrinkling analysis in this section. The film/substrate bilayer is subject to compression by a prescribed horizontal displacement ($\hat{u}$) along the right side, while the horizontal displacement is zero along the left side. The nominal compressive strain is thus, $\varepsilon = \hat{u}/L$. The shear traction is zero on both sides. The lower surface of the substrate is subject to zero normal displacement and zero shear traction, while the upper surface of the film is traction free. Both the film and the substrate are modeled by 2D quadrilateral elements (CPE8R). A uniform mesh is used for the film with at least 4 elements across the film thickness. The mesh size for the substrate is graded in the thickness direction, finer near the interface. The mesh independence of the numerical results was checked and confirmed. An alternative finite element method is described in Appendix A, in which the substrate is treated analytically as a semi-infinite half plane and the film is modeled by using one-dimensional (1D) elements. The results from both methods will be compared. For most numerical results in the present study, we set the linear elastic material properties for the film and the substrate with $E_f/E_s = 1000$ and $\nu_f = \nu_s = 1/3$. The high modulus ratio represents a typical material system with a stiff skin layer on a soft substrate (Mei et al., 2007).

A linear eigenvalue analysis is performed with the finite element model to predict the critical strain for onset of wrinkling and the corresponding eigenmode. To compare with the analytical solution for an infinitely thick substrate, we examine the effect of the substrate thickness (H) in the finite element model and use a sufficiently large thickness for the subsequent analysis. Fig. 4a shows the

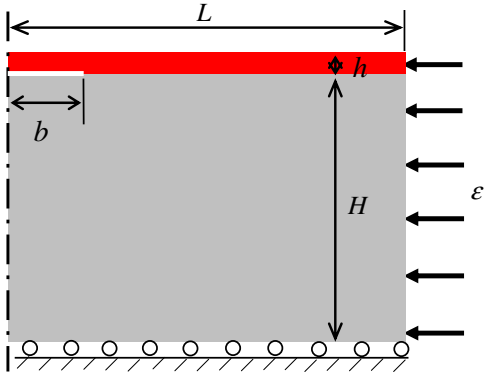

Fig. 3. Schematic illustration of the finite element model for wrinkling and buckle-delamination.

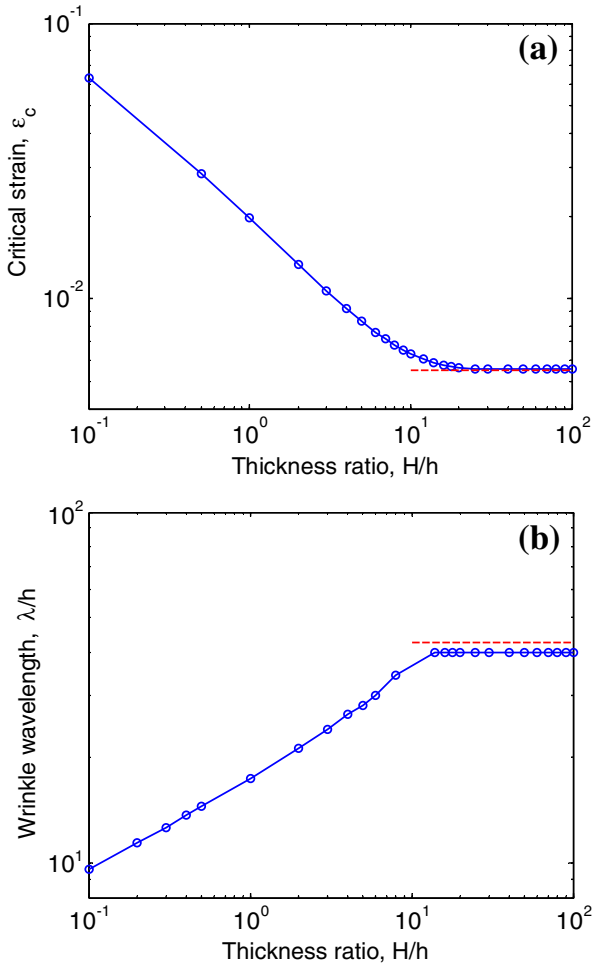

Fig. 4. Effect of substrate thickness on the finite element analysis of wrinkling: (a) critical strain; (b) wrinkle wavelength. The material properties are $E_f/E_s = 1000$, and $\nu_f = \nu_s = 1/3$. The horizontal dashed lines indicate the analytical solutions for an infinitely thick substrate.

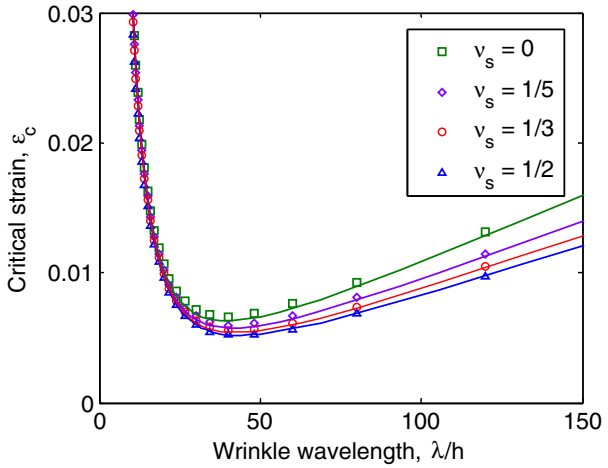

Fig. 5. Critical strain for wrinkling from the finite element eigenvalue analysis, in comparison with the analytical solution in (11), with $E_f/E_s = 1000$ and $\nu_f = \nu_s$.

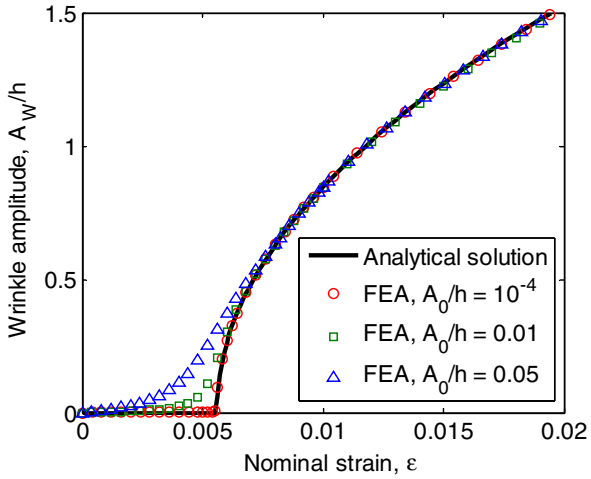

Fig. 6. Wrinkle amplitude as a function of the nominal strain, comparing the results from post-buckling finite element analysis with the analytical solution in (14) for $E_f/E_s = 1000$ and $\nu_f = \nu_s = 1/3$.

critical strain as a function of H by the finite-element eigenvalue analysis, and Fig. 4b shows the corresponding wrinkle wavelength of the eigenmode. Both the critical strain and the wrinkle wavelength become independent of the substrate thickness for $H > 20h$, while the wrinkle wavelength is about $40h$. Similar thickness effect was predicted by an analytical model (Huang et al., 2005). To simulate an infinitely thick substrate, we set $H = 100h$ in the 2D finite element model unless noted otherwise.

Fig. 5 compares the FEA results with the analytical solution in (11) for different values of Poisson's ratio (ν_s). Each eigenvalue analysis predicts a set of eigenvalues and eigen modes, based on which the critical strain for each eigenmode of a particular wavelength is obtained. To satisfy the prescribed boundary conditions, the wavelengths of permissible eigen modes take discrete values such that $L/\lambda = n/2$ ($n = 1, 2, \ldots$). For a finite length L, e.g., $L = 120h$ in the present model, the critical strain is obtained as discrete points in Fig. 5. On the other hand, the analytical solution for the critical strain in (11) is plotted as continuous solid lines. The numerical results agree closely with the analytical solution, showing an appreciable dependence on Poisson's ratio. In particular, for $\nu_s = \nu_f = 1/3$, the minimum critical strain predicted by the analytical solution in (13) is $\varepsilon_c^{**} = 0.00543$ and the corresponding wrinkle wavelength is $\lambda^{**} = 42.6h$. With a discrete set of eigen modes for the finite element model, the wavelength of the first eigen mode is $\lambda = 40h$, with the critical strain $\varepsilon_c = 0.00556$. Due to the slightly different wavelength, the minimum critical strain obtained by FEA is slightly higher than the analytical solution. The agreement can be improved by using a larger value of L or by choosing L to be a multiple of the predicted wrinkle wavelength (λ^{**}). The results from the 2D and 1D finite element methods are practically indistinguishable for the eigenvalue analysis.

To simulate wrinkle growth beyond the critical strain, a nonlinear post-buckling analysis is performed with the 2D finite element model. The first eigenmode obtained from the linear analysis is used as the initial geometric imperfection to trigger buckling instability. Fig. 6 shows the wrinkle amplitude as a function of the nominal strain. For comparison, the approximate analytical solution in (14) is plotted as a continuous solid line with $\lambda = 40h$ and $\varepsilon_c = 0.00556$ for the first eigenmode. The numerical results vary slightly as the amplitude of the initial imperfection (A_0/h) varies. The onset of wrinkling at the critical strain becomes less abrupt if the amplitude of the initial imperfection is relatively large. Using a small initial imperfection ($A_0/h = 10^{-4}$), the numerical results compare closely with the analytical solution, with an abrupt transition at the critical strain. In the 1D finite element model, instead of the geometric imperfection, we introduce a displacement perturbation for the post-buckling analysis, and the wrinkle amplitude is found to be in excellent agreement with the analytical solution with no dependence on the perturbation amplitude. It is thus concluded that the analytical solution (14) is a good approximation for the wrinkle amplitude as long as the critical strain and the wrinkle wavelength are used accurately. By setting $\lambda = \lambda^{**}$ and $\varepsilon_c = \varepsilon_c^{**}$ in (14), we obtain that

$$A_W^{**} = h\sqrt{\frac{\varepsilon}{\varepsilon_c^{**}} - 1}. \tag{16}$$

The effect of the substrate Poisson's ratio on the wrinkle amplitude is thus fully accounted for by using the critical strain in (13) instead of (3).

2.3. Wrinkle-induced delamination

As the wrinkle amplitude grows, the normal and shear tractions acting on the film/substrate interface increase, which may cause delamination (Shield et al., 1994; Liang et al., 2002; Mei et al., 2007; Goyal et al., 2010). To estimate the interfacial tractions in the nonlinear post-buckling regime, we assume zero tangential displacement in (6) so that the maximum shear traction is linearly related to the maximum normal traction, namely

$$\tau_m = -\frac{1-2\nu_s}{2(1-\nu_s)} q_m. \tag{17}$$

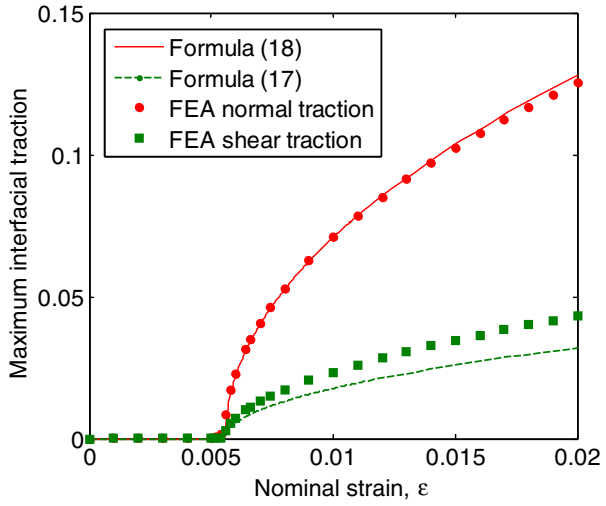

Fig. 7. The maximum normal and shear tractions at the film/substrate interface, in comparison with the analytical solutions in (17) and (18). The tractions are normalized by the substrate modulus $\overline{E}_s$.

Inserting (17) into (7) along with (14) for the wrinkle amplitude, we obtain the maximum normal traction as a function of the nominal strain:

$$q_m = \frac{4(1-\nu_s)^2\overline{E}_s}{3-4\nu_s}\sqrt{\varepsilon-\varepsilon_c}. \tag{18}$$

Alternatively, the normal traction may be estimated by assuming zero shear traction in (7). By comparing to the FEA results, as shown in Fig. 7, it is found that the zero tangential displacement assumption offers a better approximation for estimating the wrinkle-induced tractions at the interface. The maximum normal traction by FEA follows (18) remarkably well. While the formula in (17) underestimates the maximum shear traction, it is clear that the shear traction is not zero at the interface.

The close agreement for the maximum normal traction in Fig. 7 suggests that the formula (18) may be used as a good approximation to estimate the critical strain for initiation of wrinkle-induced interfacial delamination. In a separate study using a cohesive zone model (Mei, 2011), it is found that initiation of delamination is predominantly determined by the strength of the interface subject to the normal traction. Similar results have been reported by Goyal et al. (2010). By setting the maximum normal traction in (18) equal the interfacial strength ($\hat{\sigma}_{\text{int}}$), we obtain the critical strain for initiation of wrinkle-induced delamination (WID), namely

$$\varepsilon_{WID} = \varepsilon_c + \left(\frac{3-4\nu_s}{4(1-\nu_s)^2}\frac{\hat{\sigma}_{\text{int}}}{\overline{E}_s}\right)^2, \tag{19}$$

where ε_c is the critical strain for wrinkling with no delamination as given in (10), and $\hat{\sigma}_{\text{int}}$ is the peak stress in the normal traction–separation relation for the interface as described by a cohesive zone model (Hutchinson and Evans, 2000). Beyond the critical strain ε_{WID}, the interfacial delamination grows concomitantly with wrinkling. As a result, the two buckling modes, wrinkling with no delamination and buckle-delamination, may co-exist and interact with each other.

3. Onset of buckling, with delamination

For a thin film bonded to a stiff substrate, wrinkling is unlikely, due to the effect of substrate constraint that requires a high critical strain for wrinkling without delamination. However, with defects at the film/substrate interface, such as partial delamination of the film, buckling of the film under compression may occur, which in turn drives growth of delamination (Fig. 1b), known as buckle-delamination (Hutchinson and Suo, 1992; Ortiz and Gioia, 1997; Moon et al., 2002). For a compliant substrate, with the presence of interfacial delamination, both wrinkling and buckle-delamination are possible and they may co-exist (Mei et al., 2007; Nolte et al., submitted for publication). In this section, we discuss the effect of pre-existing interfacial delamination on the critical strain for buckling and transition of the initial buckling mode.

Early studies of buckle-delamination often assumed a fixed-end condition at the edge of delamination, which essentially neglected the effect of elastic deformation in the substrate (Hutchinson and Suo, 1992). Under such a condition, the critical strain for onset of buckling is identical to that for a freestanding sheet with clamped edges, namely

$$\varepsilon_B = \frac{\pi^2}{12}\left(\frac{h}{b}\right)^2, \tag{20}$$

where b is the half-width of the delamination (see Fig. 1b).

Recent studies (Cotterell and Chen, 2000; Yu and Hutchinson, 2002; Parry et al., 2005) have shown that the critical strain for buckling can be significantly lower than that predicted by (20) when elastic deformation of the substrate is taken into account, especially for relatively compliant substrates. By a semi-analytical approach, Yu and Hutchinson (2002) derived an implicit formula for the critical strain of buckling (ε_B^*):

$$\sqrt{\frac{\varepsilon_B}{\varepsilon_B^*}}\tan\left(\pi\sqrt{\frac{\varepsilon_B^*}{\varepsilon_B}}\right) = \frac{\pi h}{12b}\left(\frac{a_{12}^2}{a_{11}+b/h}-a_{22}\right). \tag{21}$$

The dimensionless coefficients a_{ij} in (21), which depend on the ratio b/h and the elastic mismatch between the film and the substrate, are determined numerically, either by solving an integral equation or by finite element calculations. In the present study, a finite element method is used to calculate these coefficients as summarized in Appendix B. Table 1 lists the values of these coefficients for $E_f/E_s = 1000$ and $\nu_f = \nu_s = 1/3$.

Table 1
Coefficients a_{ij} for $E_f/E_s = 1000$ and $\nu_f = \nu_s = 1/3$.

b/h	1	5	10	20	50
a_{11}	467.12	604.88	691.77	807.32	1028.55
a_{22}	78.23	75.23	74.57	74.29	74.18
$a_{12} = a_{21}$	27.71	20.72	17.77	15.32	12.83
a_{31}	409.77	404.63	391.65	373.58	357.94
a_{32}	319.08	279.43	262.41	252.51	248.50

The above semi-analytical solution has two limitations. First, the delamination size must be much larger than the film thickness so that the beam equations are applicable for the delaminated film segment. Second, the buckling mode is prescribed as the localized buckle-delamination, which may not be the critical mode for a very compliant substrate. By introducing an interfacial crack in the 2D finite element model (Fig. 3), we perform a linear eigenvalue analysis to predict the critical strain for onset of buckling with delamination. By symmetry, only half of the delamination crack is modeled. Here, since the film is modeled by 2D solid elements, relatively short interfacial cracks can be considered. Moreover, the buckling mode is not prescribed in the finite-element eigenvalue analysis, which searches for all possible eigen modes that satisfy the boundary conditions. The eigenvalue for the first eigen mode gives the critical strain for onset of buckling instability.

Fig. 8 shows the results from two sets of the finite element analysis (FEA). First, for $E_f/E_s = 1000$, the critical strain is obtained as a function of b/h. Second, for $b/h = 10$, the critical strain is calculated as a function of E_f/E_s. In both cases, $\nu_f = \nu_s = 1/3$. Remarkably, the numerical results collapse onto one single curve in Fig. 8, where the critical strain is scaled by ε_c^{**}, the critical strain for wrinkling as given in Eq. (13), and the delamination width is scaled by λ^{**}, the wrinkle wavelength in Eq. (12). For comparison, the analytical solution in (20) and the semi-analytical solution in (21) are plotted in the same manner. Thus, the critical strain for onset of buckling can be written in a compact form

$$\frac{\varepsilon_B^{**}}{\varepsilon_c^{**}} = f\left(\frac{b}{\lambda^{**}}\right), \tag{22}$$

which takes into account both the effect of delamination width and the effect of elastic mismatch on the critical strain.

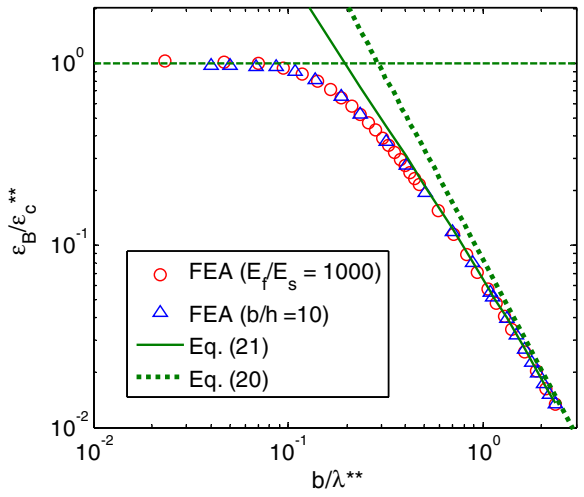

Fig. 8. Comparison of the critical strain for buckling between analytical solutions and the finite-element eigenvalue analysis. The open circles are for $E_f/E_s = 1000$ with varying b/h, and the open triangles are for $b/h = 10$ with varying E_f/E_s. The critical strain for wrinkling (ε_c^{**}) and the wrinkle wavelength (λ^{**}) are used to scale the critical strain and the delamination width.

As shown in Fig. 8, the FEA results agree closely with the prediction by (21) for relatively large delamination width (e.g., $b/\lambda^{**} > 0.5$). Both the FEA results and the semi-analytical solution approach the analytical solution in (20) when $b/\lambda^{**} > 2$. For relatively short delamination cracks, however, the FEA results deviate from the semi-analytical solution. As b/λ^{**} decreases, the FEA-predicted critical strain approaches a plateau that corresponds to the critical strain for wrinkling with no delamination, i.e., $\varepsilon_B^{**}/\varepsilon_c^{**} \to 1$. Fig. 9 shows the eigen modes for three different delamination widths with $E_f/E_s = 1000$, which reveals a transition from the localized mode of buckle-delamination to the periodic wrinkling mode. When b/h is large, buckling occurs predominantly at the location of delamination. When b/h is small, buckling is not restricted to the delaminated part and periodic wrinkles form. The smooth transition of the critical strain shown in Fig. 8 suggests that a mixed mode of buckling occurs with an intermediate delamination length ($0.1 < b/\lambda^{**} < 0.5$), for which the analytical solutions for both buckle-delamination and wrinkling overestimate the critical strain. The results from the 1D finite element model (Appendix A) are in close agreement with the 2D FEA results.

4. Post-buckling analysis with delamination

Beyond the critical strain, the buckle amplitude increases with the nominal strain, and the delamination crack may grow. For an elastic film on a rigid substrate, the buckle amplitude is obtained analytically (Chai et al., 1981; Hutchinson and Suo, 1992) as

$$A_B = \frac{2h}{\sqrt{3}}\sqrt{\frac{\varepsilon}{\varepsilon_B} - 1}, \tag{23}$$

where ε_B is the critical strain for onset of buckling as given in (20). The energy release rate driving growth of the interfacial delamination is

$$G = G_0\left(1 - \frac{\varepsilon_B}{\varepsilon}\right)\left(1 + \frac{3\varepsilon_B}{\varepsilon}\right), \tag{24}$$

where $G_0 = \bar{E}_f h\varepsilon^2/2$. The delamination grows when the energy release rate exceeds the interfacial toughness and arrests when it drops below the toughness.

For an elastic compliant substrate, both the buckle amplitude and the energy release rate can be significantly greater than the predictions by the rigid-substrate model (Cotterell and Chen, 2000; Yu and Hutchinson, 2002; Parry et al., 2005). Following Yu and Hutchinson (2002), a semi-analytical approach is summarized in Appendix B, which takes into account the effects of substrate compliance on the buckle amplitude and energy release rate. However, as discussed in Section 3, the semi-analytical approach tends to overestimate the critical strain for onset of buckling, which in turn affects the prediction of post-buckling behavior, especially for relatively short cracks and very compliant substrates. Using the finite element model with delamination (Fig. 3), we perform a nonlinear post-buckling analysis to study the evolution of the buckling mode beyond the critical strain. The eigenmode obtained by the

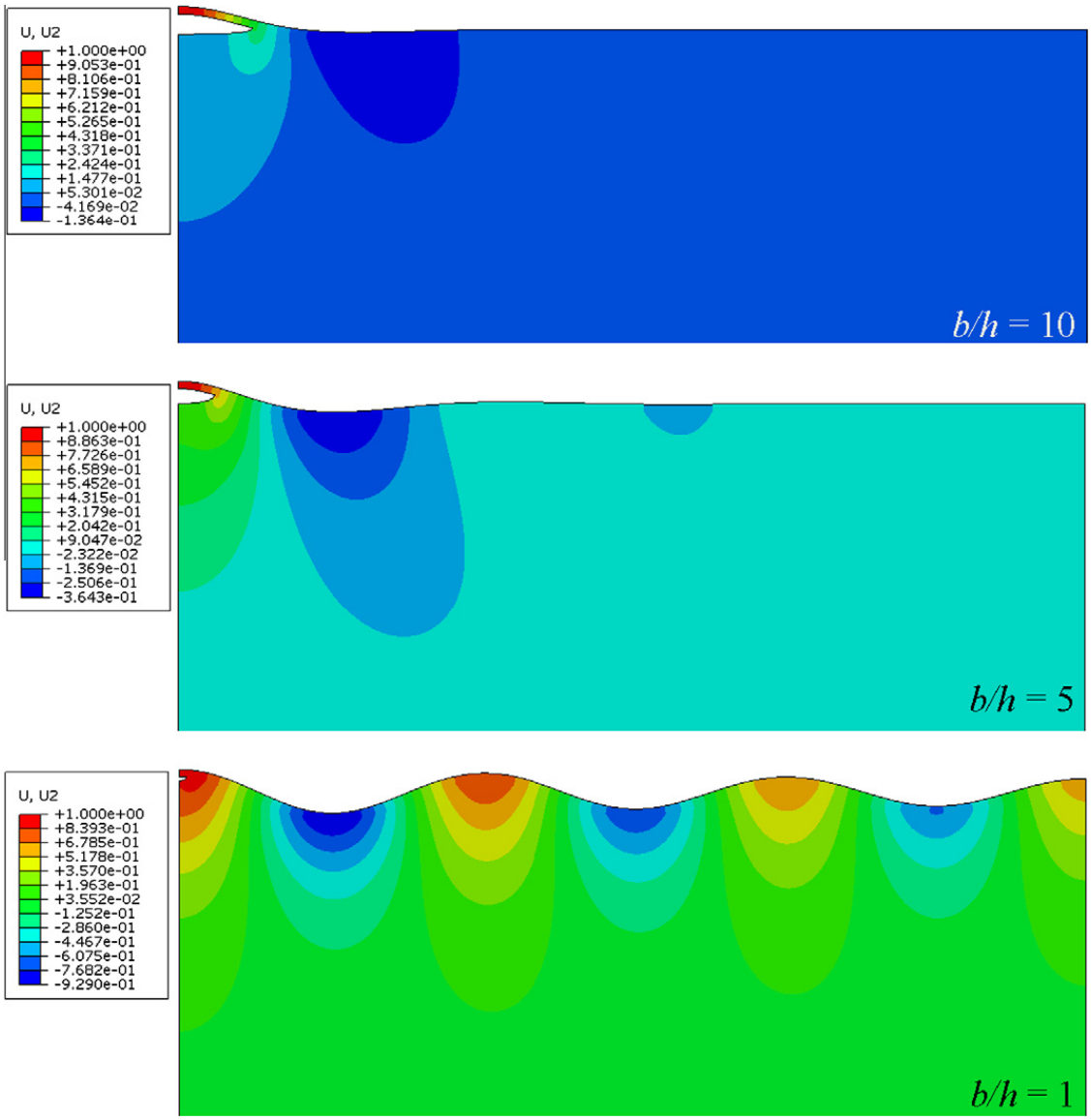

Fig. 9. Eigen modes of an elastic thin film on an elastic compliant substrate with pre-existing interfacial delamination of different sizes (b/h = 10, 5, and 1).

linear analysis in Section 3 is used as the initial imperfection with a small amplitude ($A_0/h = 10^{-4}$).

Fig. 10a shows the evolution of the buckling profile as the nominal strain increases. For b/h = 10, the critical strain predicted by the eigenvalue analysis is 0.00284. The film remains flat when $\varepsilon < 0.00284$. Beyond the critical strain, the buckling deformation is predominantly localized near the location of delamination, and the film remains flat far away from the delamination. As the film buckles, the substrate surface is pulled up significantly near the edge of delamination, as shown by the dashed lines. The film deforms with both out-of-plane displacement and rotation at the edge of delamination. Beyond the edge, the film first bends down and then up, forming a valley before it becomes nearly flat. Far away from the delamination, the film and the substrate surface moves up slightly due to Poisson's effect. We define the buckle amplitude A_B as the difference between the vertical displacement at the peak and that at the valley. Fig. 10b plots the buckle amplitude as a function of the nominal strain for b/h = 1, 5, 10, and 20. As b/h increases, the critical strain for onset of buckling decreases, and the buckling amplitude increases. For small b/h, the buckling profile becomes periodic wrinkles, and as expected the buckle amplitude approaches twice the wrinkle amplitude predicted by the analytical solution in (14). It is noted that the presence of even a short interfacial delamination could raise the apparent wrinkle amplitude beyond the analytical prediction.

It is found that the results from the post-buckling analysis strongly depend on the ratio, L/b, in the finite element model. As shown in Fig. 11a, the buckle amplitude increases with increasing L/b, while the critical strain for onset of buckling is independent of L/b. Correspondingly, the energy release rate for buckle-driven delamination, calculated by the method of J-integral (Rice, 1968), also increases as L/b increases (Fig. 11b). For comparison, the rigid-substrate solutions in (23) and (24) are plotted as the thick dashed lines, and the semi-analytical solutions

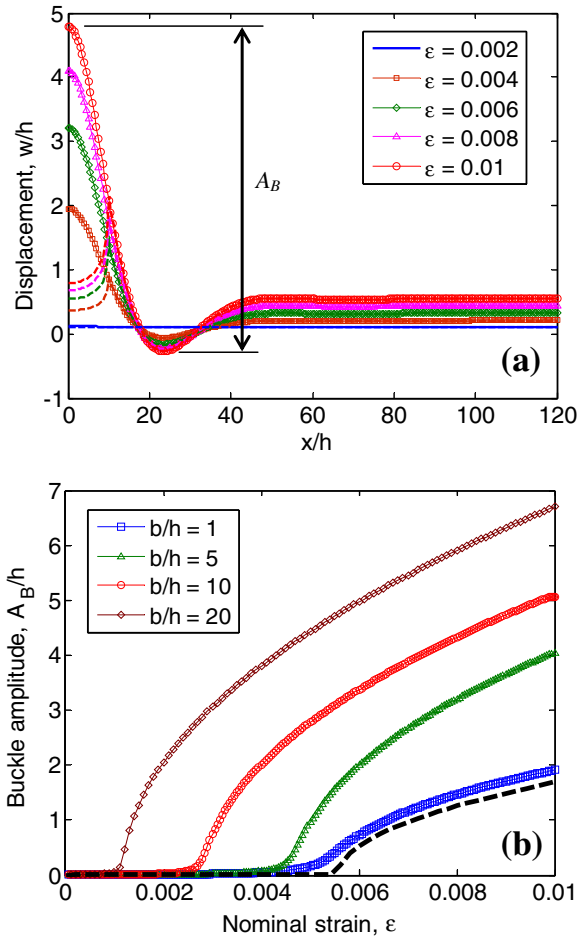

Fig. 10. (a) Out-of-plane displacements of the film (solid lines) and the substrate surface (dashed lines) by the post-buckling finite element analysis for $b/h = 10$ and $L/h = 120$. (b) Buckle amplitude as a function of the nominal strain for different b/h. The dashed line in (b) shows twice of the wrinkle amplitude with no delamination as predicted by the analytical solution in (14).

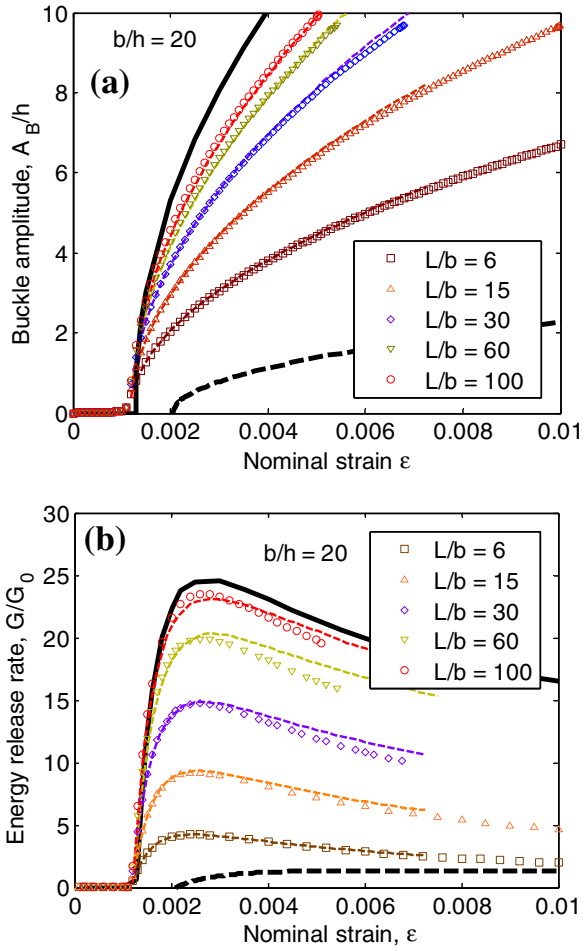

Fig. 11. (a) Buckle amplitude and (b) energy release rate for $b/h = 20$. Two different finite element models are used and compared along with the semi-analytical solution (thick solid lines). The results from the 2D model are the open symbols, and those from the 1D model are the dashed lines. The thick dashed lines are the rigid-substrate solution in (23) and (24).

by Yu–Hutchinson approach are plotted as the thick solid lines. It is expected that the FEA results eventually converge towards the semi-analytical solution for a sufficiently large L/b. Such convergence can be easily achieved for a relatively stiff substrate (e.g., $E_f/E_s < 100$). For a compliant substrate, however, the convergence can be very slow. Fig. 12 shows the energy release rate, normalized by the semi-analytical solution (G_∞), as a function of L/b for different modulus ratios. For $E_f/E_s = 100$, the calculated energy release rate agrees closely with G_∞ for $L/b = 60$ and beyond. With $E_f/E_s = 1000$, the convergence is not reached for L/b up to 100. Such a slow convergence may be qualitatively understood as the shear-lag effect. The stress in the film is partly relaxed by buckling at the delamination but unaffected far away from the delamination. In between, the stress in the film varies over a characteristic length scale for load transfer, depending on the stiffness of the substrate as defined in a shear lag model (Xia and Hutchinson, 2000). The length scale is much longer for a compliant substrate than for a stiff substrate. For the finite element model with L smaller or comparable to the shear lag length, due to interaction between buckle-delamination

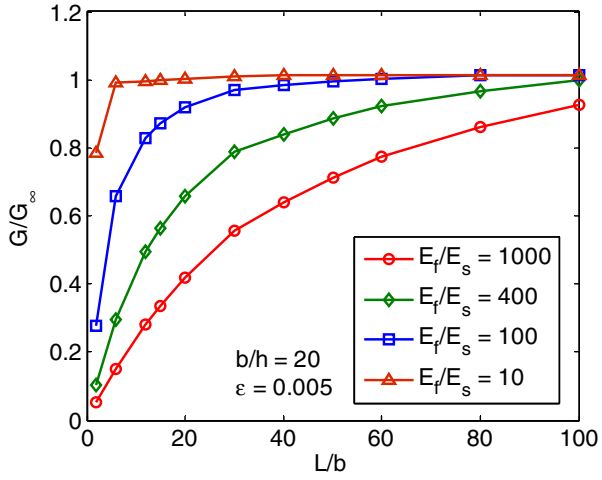

Fig. 12. Dependence of the energy release rate for buckle-delamination on the length ratio (L/b) and the modulus ratio (E_f/E_s).

at one end of the film and the boundary conditions at the other end, both the buckle amplitude and the energy

release rate depend on L. Alternatively, the results in Figs. 11 and 12 may be understood as the post-buckling behavior for a periodic array of buckle-delamination with a spacing $2(L-b)$ between the adjacent delamination cracks, for which the effect of spacing is similar to that for a periodic array of channeling cracks in an elastic thin film on a compliant substrate (Xia and Hutchinson, 2000; Huang et al., 2003).

The thickness of the substrate in the 2D finite element model must be sufficiently large to simulate an infinitely thick substrate. As shown in Fig. 4, the thickness ratio $H/h = 100$ is sufficient for the wrinkling analysis. For buckling with delamination, the thickness ratio depends on the delamination size, and $H/h = 200$ is found to be sufficient for b/h up to 50 in the present study. For comparison, the results from the 1D finite element method (Appendix A) are shown in Fig. 11, in which the substrate is modeled exactly as an infinite half plane. The results from both finite element methods are in close agreement for the wrinkling analysis and for the eigenvalue analysis of buckling with delamination. For the post-buckling analysis, the two methods agree closely for the buckle amplitude but differ slightly for the energy release rate. The discrepancy may be attributed to the calculation of the J-integral with different models for the film (i.e., 2D solid elements vs 1D beam elements) and for the substrate (i.e., finite thickness vs infinite).

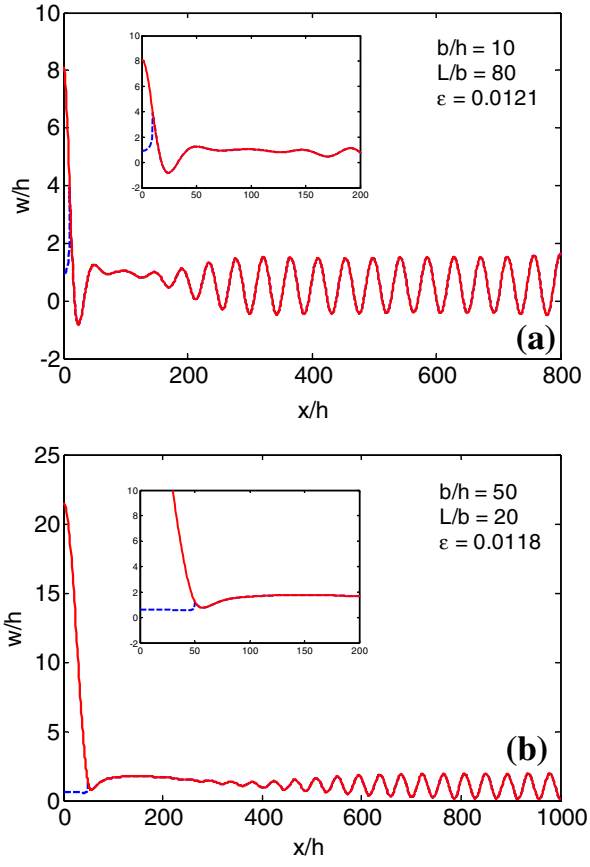

Fig. 13. Concomitant wrinkling and buckle-delamination of a thin film on a compliant substrate ($E_f/E_s = 1000$) with (a) $b/h = 10$ ($L/h = 800$) and (b) $b/h = 50$ ($L/h = 1000$). The dashed line indicates the substrate surface. The insets show the local view near the edge of delamination.

For a very compliant substrate, it is found that localized buckle-delamination and periodic wrinkles may coexist when L/b is sufficiently large. Fig. 13 shows two examples, one for $b/h = 10$ and the other for $b/h = 50$. In both cases, the onset of buckle-delamination occurs first, followed by formation of periodic wrinkles. The buckle amplitude is much larger than the wrinkle amplitude, and the film is nearly flat in a region between buckle-delamination and periodic wrinkles. The wrinkle wavelength agrees closely with the prediction by the analytical solution in (12). Fig. 14 shows the surface contours for $b/h = 50$ at two different strain levels, mimicking what may be observed in experiments by an optical micrograph (Nolte et al., submitted for publication). When the nominal strain is low, only the localized buckle is observable at the location of pre-existing delamination. At a higher strain, periodic wrinkles form at a distance away from the delamination. Between the wrinkles and buckle-delamination is a region of interaction, where the compressive stress in the film is partly relaxed by buckle-delamination at one side and by wrinkling at the other side. The stress varies over a distance that depends on the size of delamination (b/h) as well as the substrate compliance by the shear lag effect. The stress variation is reflected by the variation of the wrinkle amplitude from zero to nearly constant (Fig. 13). We note that the numerical results (e.g., buckle amplitudes) depend on the model size (L/b) due to the long shear-lag length of interaction for the compliant substrate in these simulations, but the characteristics of the interaction between the two buckling modes shall remain the same as long as L/b is sufficiently large for both buckling modes to coexist.

Fig. 15a plots the buckle amplitude as a function of the nominal strain for the case with $b/h = 50$ and $L/b = 20$, and Fig. 15b plots the energy release rate for growth of the delamination. The critical strain for onset of buckling in this case is very small ($\sim$0.00026). Beyond the critical strain, the buckle amplitude and the energy release rate increase. For comparison, the rigid-substrate solution in (23) and (24) are plotted as the thick dashed lines, and the semi-analytical solutions by the Yu–Hutchinson approach are plotted as the thick solid lines. Both the buckle amplitude and the energy release rate by the finite element model are lower than the semi-analytical solution, because the ratio $L/b = 20$ is not large enough to simulate an infinite substrate as assumed by the semi-analytical solution. Furthermore, when the nominal strain reaches around 0.0092, both the buckle amplitude and the energy release rate stop increasing. This change of behavior coincides with the onset of wrinkling away from the delamination (Fig. 15a). On the other hand, we note that the nominal strain for onset of wrinkling is greater than the analytical prediction by (13). Therefore, while the growth of wrinkling reduces the buckle amplitude and the energy release rate, the presence of buckle-delamination delays onset of wrinkling. With a very compliant substrate, the two buckling modes interact over a long range with a length scale more than three orders of magnitude greater than the film thickness.

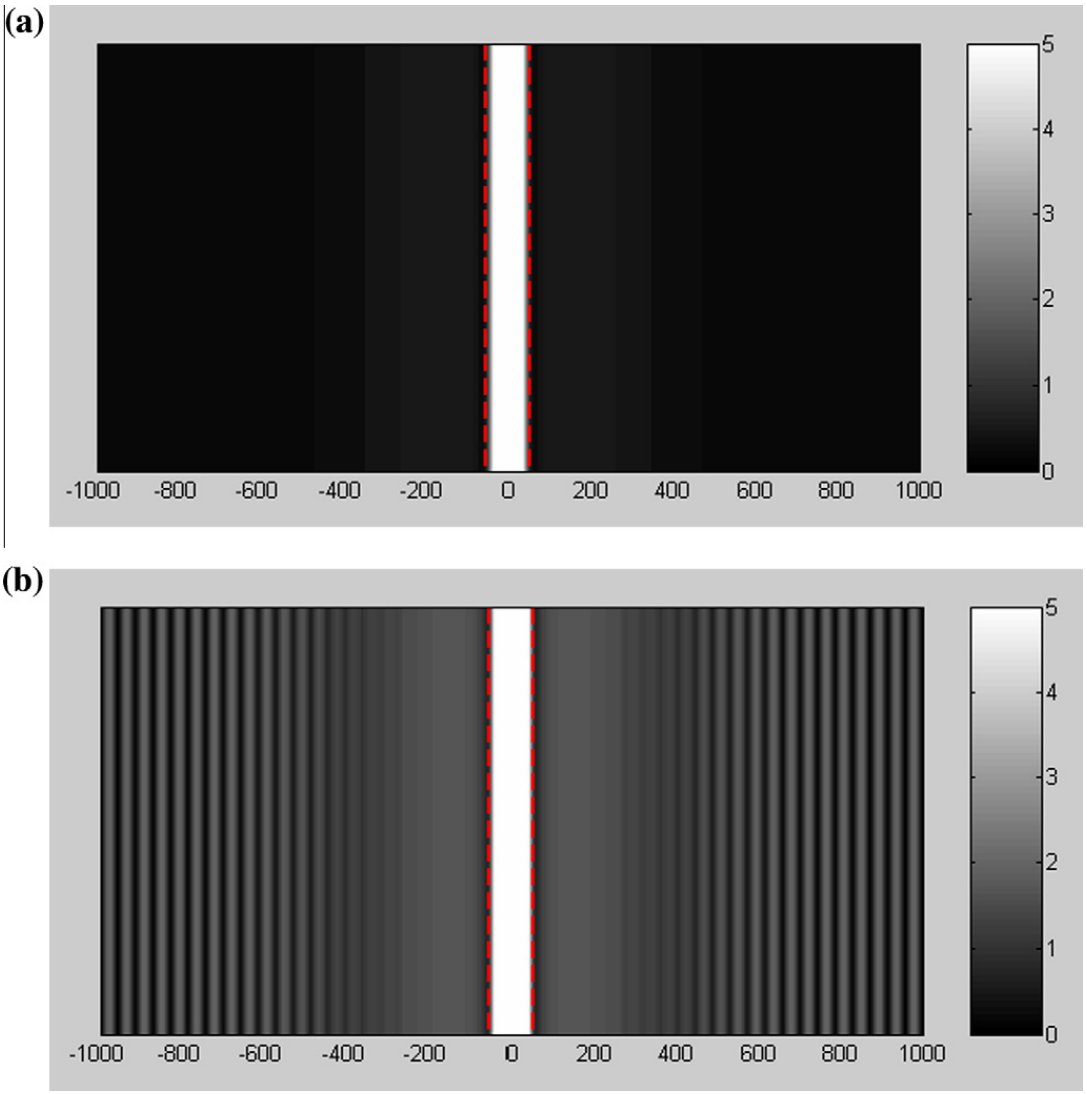

Fig. 14. Gray-scale contour plots of the surface profiles for $b/h = 50$ at two different strain levels: (a) $\varepsilon = 0.0032$; (b) $\varepsilon = 0.0118$. The red dashed lines indicate the edges of delamination. (For interpretation of the references to color in this figure legend, the reader is referred to the web version of this article.)

5. Discussions

5.1. Co-evolution of wrinkling and buckle-delamination

In the present study, we have considered two scenarios for concomitant wrinkling and buckle-delamination of an elastic thin film on a compliant substrate under compression. First, if the film/substrate interface is perfectly bonded, wrinkling occurs beyond a critical strain. Subsequently, nucleation of interfacial delamination may occur at a larger nominal strain when the wrinkle-induced normal traction at the interface exceeds the strength of the interface. The growth of the interfacial delamination however requires further studies, for which a cohesive zone model may be adopted for the interface (Goyal et al., 2010). Second, with pre-existing interfacial delamination, the initial buckling mode depends on the size of the pre-existing delamination. With a relatively large delamination, localized buckle-delamination occurs first, followed by wrinkling away from the delamination. Again, the growth of interfacial delamination is not considered in the present study, but the critical condition for the pre-existing delamination to grow may be predicted by comparing the energy release rate with the interface toughness. These two scenarios qualitatively agree with the experimental observations (Mei et al., 2007; Nolte et al., submitted for publication).

Two failure criteria are suggested for hybrid systems with stiff thin films on compliant substrates. First, for applications that require perfect bonding at the interface, the strength criterion may be used to determine the critical nominal strain for wrinkle-induced nucleation of interfacial delamination, as given in Eq. (19). Second, to prevent pre-existing delamination from growing, the toughness criterion may be used by comparing the calculated energy release rate with the interface toughness (or adhesion energy). It is shown that the calculation of the energy release rate is sensitive to the substrate size, especially for a very compliant substrate. Moreover, the growth of wrinkling away from the delamination can significantly affect the

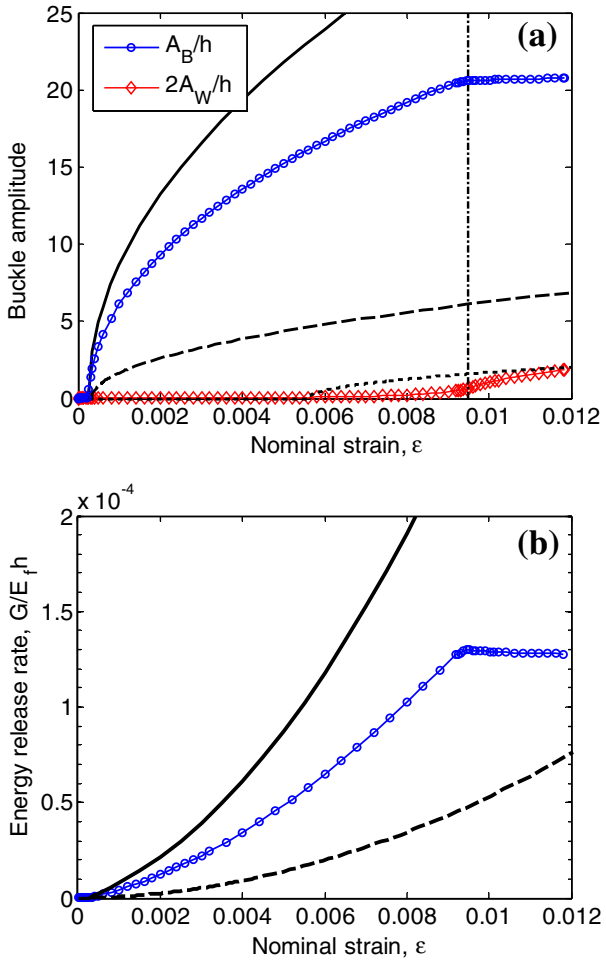

Fig. 15. (a) Amplitudes of buckling and wrinkling for $b/h = 50$ ($L/b = 20$ and $H/h = 200$). (b) Energy release rate for delamination. The thick solid lines are the semi-analytical solution, and the thick dashed lines are the rigid-substrate solution in (23) and (24). The thick dotted line in (a) is twice the wrinkle amplitude by (16) assuming no delamination.

energy release rate and thus the growth of delamination. It seems possible that in some cases the pre-existing delamination could be pinned by the wrinkles, as the energy release rate stops increasing once wrinkles start to grow (Fig. 15b). However, it is cautioned that, since both the wrinkling and buckle-delamination are highly nonlinear processes, many metastable equilibrium states may exist and snap-through instability may occur during co-evolution, posing challenges for numerical simulations.

5.2. Implications on thin film and interface metrology

It has been suggested that the phenomena of wrinkling and buckle-delamination may offer a convenient method to measuring elastic properties of thin film materials (Chung et al., 2011) as well as adhesion energy of the interface (Vella et al., 2009; Aoyanagi et al., 2010). Based on the present study, we would make the following comments.

- The wrinkle wavelength is a reliable quantity for the measurement of elastic properties, as long as the nominal strain is within the limit of linear elasticity. Unless the substrate is nearly incompressible ($\nu_s \sim 0.5$), the effect of Poisson's ratio should be taken into account by using Eq. (12) instead of Eq. (2).
- The wrinkle amplitude is less reliable as it depends sensitively on pre-existing delamination (Fig. 10), which is often unavailable from experiments.
- To determine the interface toughness or adhesion energy from buckle-delamination, both the delamination width and the nominal strain are needed for the calculation of energy release rate, which equals the interface toughness when the delamination crack is arrested. Measurement of the buckle amplitude could help to infer one of the two quantities, but no explicit relationships are obtained for either the buckle amplitude or the energy release rate. In particular, we are not able to confirm the simple formula obtained by a scaling analysis (Vella et al., 2009).
- With concomitant wrinkling and buckle-delamination, it is possible to simultaneously determine the elastic property of the thin film and the interfacial properties. First, by measuring the wrinkle wavelength far away from the buckle-delamination, the elastic modulus of the thin film can be determined by Eq. (12), assuming that the elastic properties of the substrate are known. Second, if the critical strain for wrinkle-induced nucleation of buckle-delamination can be measured, the strength of the interface may be determined by Eq. (19). As shown by Goyal et al. (2010), the buckle amplitude increases abruptly at the critical strain, which may be practically measurable. Third, once the delamination crack has arrested at a particular strain level, the interface toughness can be determined by calculating the energy release rate with the measured delamination width and the buckle amplitude.

6. Summary

As two commonly observed buckling modes, buckle-delamination and wrinkling have been analyzed separately in previous studies. In this paper, by analytical and finite element methods, we present a study on concomitant wrinkling and buckle-delamination for an elastic thin film on a compliant substrate. First, based on an analytical solution and finite element analyses of wrinkling, an approximate formula is derived to estimate the normal traction at the interface and to predict initiation of wrinkle-induced interfacial delamination. Next, the effect of pre-existing delamination on the critical strain for onset of buckling instability is examined by finite element eigenvalue analyses, showing a smooth transition between the two buckling modes. For an intermediate delamination size, a mixed mode of buckling is predicted with the critical compressive strain lower than previous solutions for both wrinkling and buckle-delamination. Nonlinear post-buckling analyses by two different finite element methods show a significant shear-lag effect with an effective load transfer length over three orders of magnitude greater than the film thickness. Finally, concomitant wrinkling and buckle-delamination is simulated to illustrate the long-range interaction between the two buckling modes. The results are discussed in view of predicting failure

mechanisms in the hybrid systems as well as implications for thin film and interface metrology.

Acknowledgments

The authors (H.M. and R.H.) gratefully acknowledge financial supports by National Science Foundation (Grant No. 0547409) and Semiconductor Research Corporation (GRC Task ID: 1883.008).

Appendix A. A finite element method for post-buckling analysis

One of the methods to analyze the post-buckling behavior of wrinkling and buckle-delamination is based upon coupling a linear elastic semi-infinite substrate to a nonlinear beam described by the von Karman theory. Due to the nonlinearity and the coupling between the normal and transverse displacements, we must resort to numerical methods to investigate the post-buckling behavior. Since the substrate is linear elastic and the beam is represented as 1D line elements, it is possible to generate solutions to this system with a 1D mesh without a 2D finite element mesh for the substrate. To accomplish this we draw upon the work of Carka and Landis (2011) to develop the finite element equations, summarized here as follows.

The principle of virtual work for the film/substrate system is written as

$$\int (N\delta\varepsilon_{xx} + M\delta\kappa)dx + \int (\tau\delta u + q\delta w)dx = 0. \tag{A.1}$$

Here, N is the axial force in the film, M is the bending moment, u and w are the tangential and normal displacements at the film/substrate interface, $\varepsilon_{xx} = u' + (w')^2/2 - w''h/2$ is the axial strain at the mid-plane of the film, $\kappa = w''$ is the curvature, τ and q are the tangential and normal tractions at the interface. The constitutive response of the film is taken as, $N = E_f h\varepsilon_{xx}/(1-\nu_f^2)$ and $M = E_f h^3\kappa/12(1-\nu_f^2)$. The novelty of the present method is in the treatment of the second term on the left-hand side of this equation. The method is based upon the realization that the solution in the substrate can be obtained analytically as an infinite series. Specifically, the displacement and the traction at the film/substrate interface can be written in the form

$$2\mu_s u^s = \sum_{n=0}^{\infty}\{[A_n + B_n(2-2\nu_s)]\sin(n\pi x) - [C_n + D_n(2-2\nu_s)]\cos(n\pi x)\} + 2\mu_s\varepsilon x, \tag{A.2a}$$

$$2\mu_s w^s = \sum_{n=0}^{\infty}\{-[A_n - B_n(1-2\nu_s)]\cos(n\pi x) - [C_n - D_n(1-2\nu_s)]\cos(n\pi x)\}, \tag{A.2b}$$

$$\tau = \sum_{n=0}^{\infty}\{-n\pi[A_n + B_n]\sin(n\pi x) + n\pi[C_n + D_n]\cos(n\pi x)\}, \tag{A.2c}$$

$$q = \sum_{n=0}^{\infty}\{n\pi A_n\cos(n\pi x) + n\pi C_n\sin(n\pi x)\}, \tag{A.2d}$$

where μ_s is the substrate shear modulus, ν_s is the substrate Poisson's ratio, ε is the nominal strain, and A_n, B_n, C_n and D_n are unknown coefficients that must be determined by linking to the finite element solution. This link is established by enforcing the weak form of displacement continuity at the interface as,

$$\int [(u^{FE} - u^s)\delta\tau + (w^{FE} - w^s)\delta q]dx = 0. \tag{A.3}$$

Eq. (A.3) is used to relate the unknown coefficients A_n, B_n, C_n and D_n to the nodal displacements, u^J and w^J, from the finite-element solution. Note that u^{FE} and w^{FE} are interpolated from u^J and w^J through the shape functions N^J as $u^{FE} = \sum_J N^J u^J$ and $w^{FE} = \sum_J N^J w^J$. The procedure required to execute this step is detailed in Carka and Landis (2011). Ultimately the process leads to the result,

$$\int (\tau\delta u + q\delta w)dx = \{\delta\mathbf{u}^N\}^T[\mathbf{K}]\{\mathbf{u}^N\} + \{\delta\mathbf{u}^N\}^T\{\mathbf{F}^s\}, \tag{A.4}$$

where $[\mathbf{K}^s]$ is the stiffness of the semi-infinite substrate, $\{\mathbf{F}^s\}$ is a set of nodal forces associated with the nominal strain ε, and $\{\mathbf{u}^N\}$ is the array of nodal displacements. Note that the stiffness contribution relates the nodal displacements on the interface to the conjugate forces supplied by the substrate. This stiffness matrix is fully dense and symmetric.

For the buckling analysis, a standard eigenvalue analysis procedure is implemented first. A standard Newton–Raphson method is implemented to deal with the nonlinearity associated with the first term of Eq. (A.1) for post-buckling analyses. Perturbations in the initial displacement fields are introduced using the eigen modes. Unlike the geometric imperfections used in the 2D finite element model, the initial displacement perturbations do not affect the equilibrium solution. The 1D finite element method is computationally more efficient than the 2D model. In addition, it eliminates the dependence on the substrate thickness in the 2D model. On the other hand, the use of the analytical solution in (A.2) is restricted to linear kinematics for the substrate.

Appendix B. A semi-analytical approach for buckle-delamination

Following the approach by Yu and Hutchinson (2002), the plane-strain buckle-delamination problem is solved by considering two parts as illustrated in Fig. B1. The delaminated part of the film is modeled by the nonlinear von Karman plate theory, and the remaining film/substrate system is treated as a linear elasticity problem. The two parts are coupled by requiring continuity of displacements and rotation at the delamination edge.

The governing equations for the delaminated part of the film are:

$$\frac{\overline{E}_f h^3}{12}\frac{d^4w}{dx^4} + T\frac{d^2w}{dx^2} = 0, \tag{B.1}$$

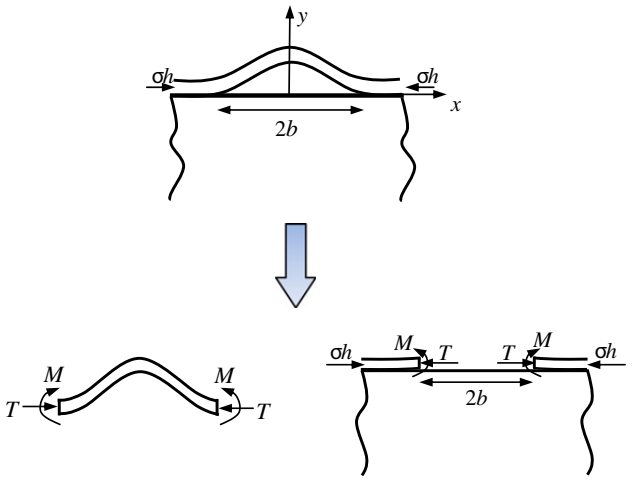

Fig. B1. Schematic illustration of the semi-analytical approach to solving the plane-strain problem for buckle-delamination.

$$\frac{du}{dx}+\frac{1}{2}\left(\frac{dw}{dx}\right)^2+\left(\frac{T}{\bar{E}_f h}-\varepsilon\right)=0, \tag{B.2}$$

where u and w are the in-plane and out-of-plane displacements of the film, ε is the nominal strain at the unbuckled state ($\varepsilon>0$ for compression), and T is the in-plane membrane force.

The boundary conditions are:

$$\left.\frac{dw}{dx}\right|_{x=0}=\left.\frac{d^3w}{dx^3}\right|_{x=0}=0 \text{ and } \left.\frac{d^2w}{dx^2}\right|_{x=b}=\frac{M}{D}, \tag{B.3}$$

where M is the bending moment at the edge of delamination and $D=\bar{E}_f h^3/12$.

Solving (B.1) and (B.2) with the boundary conditions, we obtain that

$$u(x)=\left(\varepsilon-\frac{T}{\bar{E}_f h}\right)x-\left(\frac{Mb}{2D\lambda\cos\lambda}\right)^2\left[x-\frac{b}{2\lambda}\sin\left(\frac{2\lambda x}{b}\right)\right], \tag{B.4}$$

$$w(x)=A_1-\frac{Mb^2}{D\lambda^2\cos\lambda}\cos\left(\frac{\lambda x}{b}\right), \tag{B.5}$$

where $\lambda=b\sqrt{T/D}$, and A_1 is a constant to be determined. The rotation at the edge of delamination is then

$$\theta=\left.\frac{dw}{dx}\right|_{x=b}=\frac{Mb}{D\lambda}\tan(\lambda). \tag{B.6}$$

For the remaining part of the film/substrate system, by dimensional considerations, the in-plane displacement, rotation and out-of plane displacement of the film at the edge of delamination can be written in form of

$$u(x=b)=a_{11}\frac{F}{\bar{E}_f}+a_{12}\frac{M}{\bar{E}_f h}, \tag{B.7}$$

$$\theta(x=b)=a_{21}\frac{F}{\bar{E}_f h}+a_{22}\frac{M}{\bar{E}_f h^2}, \tag{B.8}$$

$$w(x=b)=a_{31}\frac{F}{\bar{E}_f}+a_{32}\frac{M}{\bar{E}_f h}, \tag{B.9}$$

where $F=T-h\bar{E}_f\varepsilon$, and the coefficients a_{ij} are to be determined numerically. By the reciprocal theorem, $a_{21}\equiv a_{12}$.

Assuming continuity of the displacements and rotation at the edge of delamination, we combine Eqs. (B.4)–(B.9) and obtain that

$$\left(\frac{b}{h}+a_{11}\right)\frac{F}{\bar{E}_f h}+a_{12}\frac{M}{\bar{E}_f h^2}+\frac{b}{h}\left(1-\frac{\sin 2\lambda}{2\lambda}\right)\left(\frac{Mb}{2D\lambda\cos\lambda}\right)^2=0, \tag{B.10}$$

$$a_{21}\frac{F}{\bar{E}_f h}+\left(a_{22}+\frac{12b}{\lambda h}\tan\lambda\right)\frac{M}{\bar{E}_f h^2}=0, \tag{B.11}$$

$$a_{31}\frac{F}{\bar{E}_f}+\left(a_{32}+\frac{12b^2}{\lambda^2 h^2}\right)\frac{M}{\bar{E}_f h}=A_1. \tag{B.12}$$

B.1. Critical strain

Neglecting the nonlinear term, (B.10) and (B.11) form a linear eigenvalue problem, which predicts the critical condition for onset of buckling:

$$\frac{12b}{\lambda h}\tan(\lambda)=\frac{a_{12}^2}{a_{11}+b/h}-a_{22}. \tag{B.13}$$

Recall that $\lambda=b\sqrt{T/D}$. The critical membrane force T_c is determined by the critical value of λ obtained from (B.13). The critical nominal strain (ε_B^*) for onset of buckling is then predicted by the relation $T_c=\bar{E}_f h\varepsilon_B^*$. Rewriting (B.13) in terms of the critical strain, we obtain Eq. (21).

B.2. Post-buckling analysis

From (B.11), we have

$$\frac{M}{\bar{E}_f h^2}=-\frac{F}{\bar{E}_f h}\left(\frac{a_{12}}{\frac{12b}{\lambda h}\tan\lambda+a_{22}}\right). \tag{B.14}$$

Inserting (B.14) into (B.10) results in a nonlinear equation,

$$\left(\frac{b}{h}+a_{11}-\frac{a_{12}^2}{\frac{12b}{\lambda h}\tan\lambda+a_{22}}\right)+\frac{b}{h}\left(1-\frac{\sin 2\lambda}{2\lambda}\right)\left(\frac{6b}{h\lambda\cos\lambda}\right)^2\times\left(\frac{a_{12}}{\frac{12b}{\lambda h}\tan\lambda+a_{22}}\right)^2\left(\frac{\lambda^2h^2}{12b^2}-\varepsilon\right)=0, \tag{B.15}$$

from which λ can be solved as a function of ε. The membrane force T is then obtained as $\lambda=b\sqrt{T/D}$.

When $\varepsilon>\varepsilon_B^*$, it can be shown that $T<\bar{E}_f h\varepsilon$. In other words, the membrane force is partly relaxed by buckling. With $F=T-h\bar{E}_f\varepsilon$, the bending moment M is obtained from (B.14). Next, inserting (B.12) into (B.5), we obtain the buckle amplitude as

$$A=w(x=0)=ha_{31}\left(\frac{T}{\bar{E}_f h}-\varepsilon\right)+a_{32}\frac{M}{\bar{E}_f h}+\frac{M}{T}\left(1-\frac{1}{\cos\lambda}\right). \tag{B.16}$$

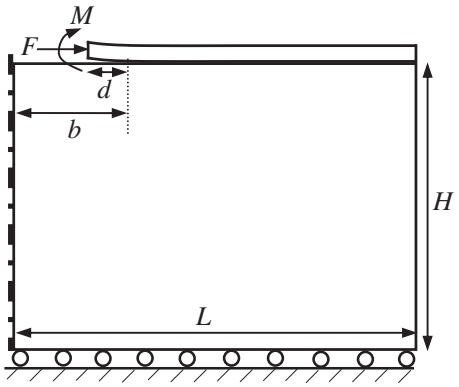

Fig. B2. Schematic of the finite element model used to calculate the coefficients a_{ij} and the energy release rate. The crack length d is zero for calculating a_{ij}. A symmetric boundary condition is assumed at the center of the delamination ($x = 0$), while the remote boundary at the right end is traction free. A mixed boundary condition is assumed at the bottom of the substrate with zero vertical displacement and zero shear traction.

B.3. Calculating the coefficients a_{ij}

To calculate the coefficients a_{ij} in (B.7), (B.8), (B.9), Yu and Hutchinson (2002) used an integral equation method. In the present study, they are calculated by a finite element method. As illustrated in Fig. B2, a 2D plane-strain finite element model is constructed using ABAQUS. To simulate a semi-infinite substrate, the thickness and length of the substrate in the finite element model must be sufficiently large. In our calculations, we set $L = H = 1000h$. The crack length d is zero for this calculation. The edge of the film at $x = b$ is subjected to an axial force F and a bending moment M. The average displacements and rotation at the edge are calculated from the nodal displacements as

$$u(x=b) = \frac{1}{h}\int u(y)dy, \tag{B.17}$$

$$\theta(x=b) = \frac{12}{h^3}\int u(y)ydy, \tag{B.18}$$

$$w(x=b) = \frac{1}{h}\int w(y)dy. \tag{B.19}$$

By applying an arbitrary force F with $M = 0$, the coefficients a_{i1} ($i = 1,2,3$) can be determined. Similarly, by applying an arbitrary moment M with $F = 0$, the coefficients a_{i2} can be determined.

B.4. Energy release rate

The energy release rate for growth of the interfacial crack may be calculated from the stress intensity factors (Yu and Hutchinson, 2002). However, the approach works only when the stress field at the crack tip exhibits the square-root singularity without oscillation (Hutchinson and Suo, 1992). For the present study, with $v_s = v_f = 1/3$, we calculate the energy release rate directly by the method of J-integral. For this purpose, a short crack ($d = h/2$) is introduced at the interface in the finite element model (Fig. B2). Quarter-point singular elements are used at the crack tip. The axial force F and the bending moment M, obtained from the post-buckling analysis in (B.15) and (B.14), are applied at the edge of the film.

References

Allen, H.G., 1969. Analysis and Design of Structural Sandwich Panels. Pergamon Press, New York.

Aoyanagi, Y., Hure, J., Bico, J., Roman, B., 2010. Random blisters on stickers: metrology through defects. Soft Matter 6, 5720–5728.

Audoly, B., Boudaoud, A., 2008. Buckling of a stiff film bound to a compliant substrate. Part I: formulation, linear stability of cylindrical patterns, secondary bifurcations. J. Mech. Phys. Solids 56, 2401–2421.

Bazant, Z., Grassl, P., 2007. Size effect of cohesive delamination fracture triggered by sandwich skin wrinkling. J. Appl. Mech. 74, 1134–1141.

Biot, M.A., 1957. Folding instability of a layered viscoelastic medium under compression. Proc. R. Soc. A 242, 444–454.

Bowden, N., Brittain, S., Evans, A.G., Hutchinson, J.W., Whitesides, G.M., 1998. Spontaneous formation of ordered structures in thin films of metals supported on an elastomeric polymer. Nature 393, 146–149.

Cai, S., Breid, D., Crosby, A.J., Suo, Z., Hutchinson, J.W., 2011. Periodic patterns and energy states of buckled films on compliant substrates. J. Mech. Phys. Solids 59, 1094–1114.

Carka, D., Landis, C.M., 2011. The Dirichlet-to-Neumann map for two-dimensional crack problems. Comput. Methods Appl. Mech. Eng. 200, 1263–1271.

Chai, H., Babcock, C.D., Knauss, W.G., 1981. One dimensional modeling of failure in laminated plates by delamination buckling. Int. J. Solids Struct. 17, 1069–1083.

Chan, E.P., Page, K.A., Im, S.H., Patton, D.L., Huang, R., Stafford, C.M., 2009. Viscoelastic properties of confined polymer films measured via thermal wrinkling. Soft Matter 5, 4638–4641.

Chan, E.P., Smith, E.J., Hayward, R.C., Crosby, A.J., 2008. Surface wrinkles for smart adhesion. Adv. Mater. 20, 711–716.

Chen, X., Hutchinson, J.W., 2004. Herringbone buckling patterns of compressed thin films on compliant substrates. J. Appl. Mech. 71, 597–603.

Chen, X., Yin, J., 2010. Buckling patterns of thin films on curved compliant substrates with applications to morphogenesis and three-dimensional micro-fabrication. Soft Matter 6, 5667–5680.

Chung, J.Y., Nolte, A.J., Stafford, C.M., 2011. Surface wrinkling: a versatile platform for measuring thin-film properties. Adv. Mater. 23, 349–368.

Cotterell, B., Chen, Z., 2000. Buckling and cracking of thin films on compliant substrates under compression. Int. J. Fract. 104, 169–179.

Genzer, J., Groenewold, J., 2006. Soft matter with hard skin: from skin wrinkles to templating and material characterization. Soft Matter 2, 310–323.

Goyal, S., Srinivasan, K., Subbarayan, G., Siegmund, T., 2010. On instability-induced debond initiation in thin film systems. Eng. Fract. Mech. 77, 1298–1313.

Groenewold, J., 2001. Wrinkling of plates coupled with soft elastic media. Physica A 298, 32–45.

Harrison, C., Stafford, C.M., Zhang, W., Karim, A., 2004. Sinusoidal phase grating created by a tunably buckled surface. Appl. Phys. Lett. 85, 4016–4018.

Huang, R., 2005. Kinetic wrinkling of an elastic film on a viscoelastic substrate. J. Mech. Phys. Solids 53, 63–89.

Huang, R., Im, S.H., 2006. Dynamics of wrinkle growth and coarsening in stressed thin films. Phys. Rev. E 74, 026214.

Huang, R., Prevost, J.H., Huang, Z.Y., Suo, Z., 2003. Channel-cracking of thin films with the extended finite element method. Eng. Fract. Mech. 70, 2513–2526.

Huang, R., Suo, Z., 2002. Instability of a compressed elastic film on a viscous layer. Int. J. Solids Struct. 39, 1791–1802.

Huang, Z.Y., Hong, W., Suo, Z., 2005. Nonlinear analysis of wrinkling in a film bonded to a compliant substrate. J. Mech. Phys. Solids 53, 2101–2118.

Hutchinson, J.W., Suo, Z., 1992. Mixed-mode cracking in layered materials. Adv. Appl. Mech. 29, 63–191.

Hutchinson, J.W., Evans, A.G., 2000. Mechanics of materials: top down approaches to fracture. Acta Mater. 48, 125–135.

Im, S.H., Huang, R., 2008. Wrinkle patterns of anisotropic crystal films on viscoelastic substrates. J. Mech. Phys. Solids 56, 3315–3330.

Jiang, H.Q., Khang, D.-Y., Song, J., Sun, Y., Huang, Y., Rogers, J.A., 2007. Finite deformation mechanics in buckled thin films on compliant supports. Proc. Natl. Acad. Sci. 104, 15607–15612.

Lacour, S.P., Jones, J., Wagner, S., Li, T., Suo, Z., 2005. Stretchable interconnects for elastic electronic surfaces. Proc. IEEE 93, 1459–1467.

Lee, D., Triantafyllidis, N., Barbar, J.R., Thouless, M.D., 2008. Surface instability of an elastic half space with material properties varying with depth. J. Mech. Phys. Solids 56, 858–868.

Liang, J., Huang, R., Yin, H., Sturm, J.C., Hobart, K.D., Suo, Z., 2002. Relaxation of compressed elastic islands on a viscous layer. Acta Mater. 50, 2933–2944.

Mei, H., Huang, R., Chung, J.Y., Stafford, C.M., Yu, H.H., 2007. Buckling modes of elastic thin films on elastic substrates. Appl. Phys. Lett. 90, 151902.

Mei, H., 2011. Fracture and Delamination of Elastic Thin Films on Compliant Substrates: Modeling and Simulations. PhD Dissertation. The University of Texas at Austin.

Moon, M.-W., Chung, J.-W., Lee, K.-R., Oh, K.H., Wang, R., Evans, A.G., 2002. An experimental study of the influence of imperfections on the buckling of compressed thin films. Acta Mater. 50, 1219–1227.

Nolte, A.J., Chung, J.Y., Stafford, C.M., 2011. Wrinkling delamination of thin polymer films on compliant substrates, submitted for publication.

Ortiz, M., Gioia, G., 1997. Delamination of compressed thin films. Adv. Appl. Mech. 33, 119–192.

Parry, G., Colin, J., Coupeau, C., Foucher, F., Cimetiere, A., Grilhe, J., 2005. Effect of substrate compliance on the global unilateral post-buckling of coatings: AFM observations and finite element calculations. Acta Mater. 53, 441–447.

Rice, J.R., 1968. A path independent integral and approximate analysis of strain concentration by notches and cracks. J. Appl. Mech. 35, 379–386.

Rogers, J.A., Someya, T., Huang, Y., 2010. Materials and mechanics for stretchable electronics. Science 327, 1603–1607.

Shield, T.W., Kim, K.-S., Shield, R.T., 1994. The buckling of an elastic layer bonded to an elastic substrate in plane strain. J. Appl. Mech. 61, 231–235.

Sun, J.-Y., Xia, S., Moon, M.-W., Oh, K.H., Kim, K.-S., 2011. Folding wrinkles of a thin stiff layer on a soft substrate, submitted for publication.

Vella, D., Bico, J., Boudaoud, A., Roman, B., Reis, P.M., 2009. The macroscopic delamination of thin films from elastic substrates. PNAS 106, 10901–10906.

Watanabe, M., Shirai, H., Hirai, T., 2002. Wrinkled polypyrrole electrode for electroactive polymer actuators. J. Appl. Phys. 92, 4631–4637.

Xia, Z.C., Hutchinson, J.W., 2000. Crack patterns in thin films. J. Mech. Phys. Solids 48, 1107–1131.

Yu, H.H., Hutchinson, J.W., 2002. Influence of substrate compliance on buckling delamination of thin films. Int. J. Fract. 113, 39–55.